ELSEVIER

Polymer 42 (2001) 6259–6270

polymer

www.elsevier.nl/locate/polymer

Atomic force microscopy investigation of filled elastomers and comparison with transmission electron microscopy — application to silica-filled silicone elastomers

F. Clément[a], A. Lapra[a], L. Bokobza[a,*], L. Monnerie[a], P. Ménez[b]

[a]*Laboratoire PCSM-UMR 7615, ESPCI, 10 rue Vauquelin, F-75231 Paris Cedex 05, France*
[b]*RHODIA Recherches, Centre de Recherches de Lyon, 85 avenue des Frères Perret, BP62, F-69192 Saint Fons Cedex, France*

Received 7 April 2000; received in revised form 29 November 2000; accepted 15 January 2001

Abstract

Tapping mode atomic force microscopy experiments were conducted on silica-filled silicone elastomers. Phase images provide a good contrast between the silicone matrix and silica structures, and allow the study of silica microdispersions. However, the phase contrast is sensitive to several experimental factors, which affect the magnitude of tip-sample interactions. The dependence of the phase contrast on the free amplitude of cantilever oscillation, on the setpoint ratio, on the cantilever stiffness and on the sample modulus was investigated. The setpoint ratio was shown to be the main parameter controlling the tip-sample force, and consequently the phase contrast. By comparing the results with transmission electron microscopy experiments, the tapping mode atomic force microscopy with phase imaging is established as an easy and powerful technique for the characterization of the silica dispersion in a silicone matrix. This study opens the way for using Atomic force microscopy to get a better understanding of reinforcement in filled rubbers.

Keywords: Atomic force microscopy; Filled elastomers; Filler dispersion

1. Introduction

The addition of active fillers into elastomers is of significant commercial importance, due to the improvement of various technical properties of the final materials. The incorporation of reinforcing particles in an elastomeric matrix increases its elastic modulus and fracture properties, such as the stress at breakage. It is well known that the reinforcing potential of a filler is dramatically dependent on the quality of its dispersion in the rubber matrix [1]. Thus, it is crucial to characterize this microdispersion. This is usually conducted by transmission electron microscopy (TEM) which reaches a sub-micron resolution [2]. However, this method requires the painful preparation of microtome sections. Atomic force microscopy (AFM), which does not require any additional preparation technique, represents an alternative method to characterize the filler microdispersion [3]. In contact mode AFM, the probe tip is mounted on a cantilever and scans the sample while maintaining contact with its surface. High pressures and lateral forces exerted on the surface by the tip can then cause irreversible damage to the sample. The method of tapping mode AFM (TMAFM) was developed to minimize sample damage during scanning. This mode is well suited to the study of soft polymers such as elastomers (Young's modulus of about 1–10 MPa).

The TMAFM experiment and phase imaging have been described in detail elsewhere [4,5]. In a few words, in tapping mode, the cantilever oscillates vertically near its resonance frequency, so that the tip makes contact with the sample surface only briefly in each cycle of oscillation. This short intermittent tip-sample contact reduces lateral forces during scanning, thus preventing sample damage. As the tip approaches the surface, the vibration characteristics of the cantilever (i.e. the amplitude, resonance frequency and phase angle of vibration) change due to the tip-sample interaction. A voltage is applied to the sample piezo by a feedback loop so that the amplitude of the cantilever oscillation remains constant. This voltage is used to generate an image of the sample topography ('Height Image'). Additionally, the phase angle with respect to the excitation piezo phase can be recorded to produce the 'Phase Image', which provides enhanced image contrasts for heterogeneous surfaces [6]. Usually, the feedback mechanism of TMAFM is controlled by the set-point ratio $r_s = A_s/A_0$, where A_0 is the amplitude of the cantilever's free

* Corresponding author. Tel.: +33-1-4079-4456; fax: +33-1-4079-4686.
E-mail address: liliane.bokobza@espci.fr (L. Bokobza).

0032-3861/01/$ - see front matter
PII: S0032-3861(01)00058-1

oscillation and A_s is the set-point amplitude maintained by adjusting the vertical position of the sample. Before any systematic study of filled elastomers by TMAFM, it is essential to investigate how image contrasts depend on experimental conditions. The images obtained from TMAFM are difficult to interpret due to the complex behavior of the driven non-linear oscillator [7,8]. This was evidenced by Magonov et al. [9]who studied the behavior of polydiethylsiloxane patches on a silicon wafer substrate by TMAFM. They found that, as the interaction between the tip and sample increased (as r_s decreased), the height contrast remained relatively constant, while phase images were observed to undergo contrast variations. In a study of Bar et al. [10], reversals in phase contrast were noted as a function of set-point ratio and free amplitude of cantilever vibration on phase separated polymer blends of poly(ethene-*co*-styrene) and poly(2,6-dimethyl-1,4-phenylene oxide). Pickering and Vancso [11] evidenced apparent contrast reversal in tapping mode height and phase images as a function of r_s on films of polystyrene-polyisoprene-polystyrene tri-block copolymer system. Basically, as Brandsch et al. [12]have evidenced, in phase imaging of polymer composites made up of rigid and compliant components, one can always find two different sets of A_0 and r_s values that lead to a reversal of image contrast. The sensitivity of the phase contrast to imaging parameters is particularly important in the case of PDMS, since the standard imaging parameters for rubbers have been determined with dienic rubbers [3,13], which have moduli substantially higher than the typical modulus of silicone elastomers.

Magonov and coworkers [9] have established very important relationships affecting phase image contrast, under the harmonic approximation, which has been shown to be valid for compliant materials such as elastomers [14–16]. They consider a freely oscillating cantilever characterized by its spring constant k, mass m, quality factor Q and resonance frequency $\omega_0 = \sqrt{\frac{k}{m}}$. The essential consequence of bringing the tip closer to the sample surface is to change the force constant of the cantilever from k to $k_{\text{eff}} = k + \sigma$, where σ is the sum of the force derivatives of all attractive and repulsive forces acting on the cantilever. When $\sigma \ll k$, the phase shift $\Delta\phi$ measured at ω_0 is given by the following relationship:

$$\Delta\phi(\omega_0) = \frac{\pi}{2} - \tan^{-1}\left(\frac{k}{Q\sigma}\right) \cong \frac{Q\sigma}{k} \tag{1}$$

$\Delta\phi$ is positive when the overall force is repulsive and negative when the overall force is attractive.

When the tip and sample come into contact and their repulsive force indents the surface, it is reasonable to approximate the overall force derivative σ by the stiffness of the tip and sample. According to the Hertz theory, this stiffness S is defined by $S = \partial F/\partial\delta = \epsilon a E^*$, where F is the force acting on the tip, δ is the indentation depth, a is the radius of the contact area A between tip and surface, ϵ is a constant and E^* is the effective modulus:

$$\frac{1}{E^*} = \frac{(1-\nu_1^2)}{E_1} + \frac{(1-\nu_2^2)}{E_2} \tag{2}$$

E_1 and E_2 are the Young's moduli, ν_1 and ν_2 are the Poisson's ratios of the tip and the sample, respectively.

Because of the temporary contact between the tip and sample surface, Eq. (1) must be written with time-averaged values $\langle\ \rangle$

$$\Delta\phi(\omega_0) \cong \langle S\rangle \frac{Q}{k} = \epsilon\langle a\rangle E^* \frac{Q}{k} \tag{3}$$

Eq. (3) shows that phase imaging can provide a map of stiffness variation on the sample surface. A stiffer region (i.e. of greater E_2) will correspond to a greater value of E^*, and of $\Delta\phi(\omega_0)$, providing the other parameters of Eq. (3) remain constant. Hence a stiffer region will appear brighter in the phase image. But this phase contrast holds only for light or moderate tapping. When tip-sample forces are greater, one must consider the effect of the contact area A. Generally, a softer material leads to a larger contact area A and a longer tip-sample contact time, because of the higher indentation depth. Consequently, a change in the stiffness S can be dominated by a change in the contact area A, and especially for high tip-sample interaction. This makes the phase shift greater on a softer than on a harder material. Thus, the phase image can undergo a contrast reversal when the imaging parameters A_0 and A_s are modified.

Therefore, it is important to examine how the phase contrast depends on these parameters, and that is what the first part of this paper is devoted to. The second part will focus on the AFM potential, compared to TEM, for a qualitative and quantitative analysis of both the silica dispersion and distribution in the PDMS matrix. This work is an important step before using AFM to study the filler dispersion in a stretched elastomer, which will help us to understand the mechanisms of reinforcement in filled rubbers. This will be the subject of a forthcoming paper.

2. Experimental section

2.1. Materials

The silica-filled silicone samples used in this study were provided by RHODIA Silicones. A PDMS gum of molecular weights $M_n = 135,000\ \text{g mol}^{-1}$ and $M_w = 390,000\ \text{g mol}^{-1}$, containing 0.078% of vinyl units, was mixed with fumed silica, at room temperature, in a 'Meili' mixer. Then, the crosslinking agent, an organic peroxide, was introduced. Finally, the compound was molded and peroxide-cured at 170°C, under a pressure of 100 bars. The networks obtained have an average molecular weight between crosslinks $M_c = 17,500\ \text{g mol}^{-1}$. All the samples studied here have the same elastomeric part but they differ

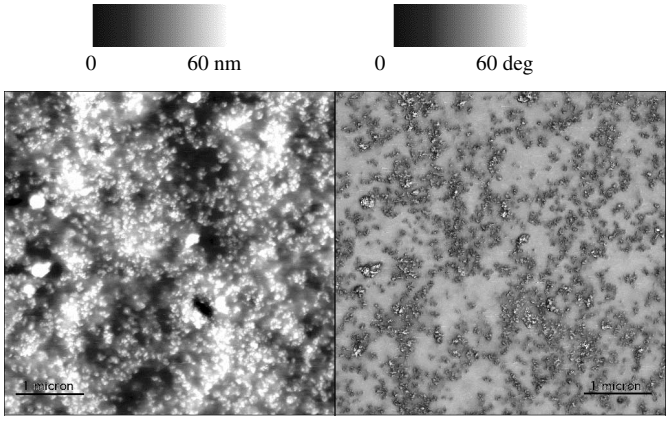

Fig. 1. Height (left) and phase (right) images of the reference system, using $A_0 = 5$ V (70 nm) and $r_s = 0.38$ ($\omega_0 = 324$ kHz).

by the silica type and/or by the silica content. The silica content is indicated in phr: parts of silica per hundred parts of rubber (by weight). Two types of silica were studied, both of them having a specific surface area of 300 $m^2\,g^{-1}$. The first one is an Aerosil® A300 provided by Degussa, and the other one is the same silica having undergone a surface treatment, performed by RHODIA Silicones, in order to improve its dispersion in the PDMS matrix. The latter will be referred as A300-t. In the rubber, silica is composed of primary structures of approximately 50 to 100 nm, which cannot be broken. These structures, called aggregates, can form larger structures (agglomerates) in the case of a poor dispersion. The samples provided are sheets, about 2 mm thick, in which we cut pieces for AFM experiments. The sample surface was not treated before the observation.

2.2. Analysis

2.2.1. Atomic force microscopy

AFM experiments were performed on a Multimode™ Nanoscope III (Digital Instruments) scanning probe microscope equipped with phase detection electronics and operating in the tapping mode under ambient conditions. We used commercial silicon (Si) cantilevers of various resonance frequencies ranging from 300 to 400 kHz. Height and phase images were recorded simultaneously at the fundamental resonance frequency of the cantilever, with a typical scan speed of 1 Hz and a resolution of 512 samples per line for a 5 μm scan size. The amplitude of oscillation at free vibration A_0 was set to values ranging from 2 to 5 V of photodiode voltage corresponding to approximately 30 to 70 nm of actual cantilever oscillation. *For all the pictures shown here, the height contrast covers height variations in the* 60 nm *range and the phase contrast covers phase angle variations in the* 60° *range. The greyscale used is the same for all the pictures.*

2.2.2. Transmission electron microscopy

The TEM experiments were performed by RHODIA Recherches on a STEM JEOL 1200EX. The filled networks were first immersed in methyl methacrylate. This immersion led to a swelling of the elastomer phase, which reached its equilibrium value within about 16 h. Thus, a polymerization was performed at 50°C during 24 h, with benzoyl peroxide. The samples obtained were then stiffer, and the thin sections required for the TEM experiments were made at room temperature. By the way, the quite tricky technique of cryo-ultramicrotoming, at a temperature lower than the

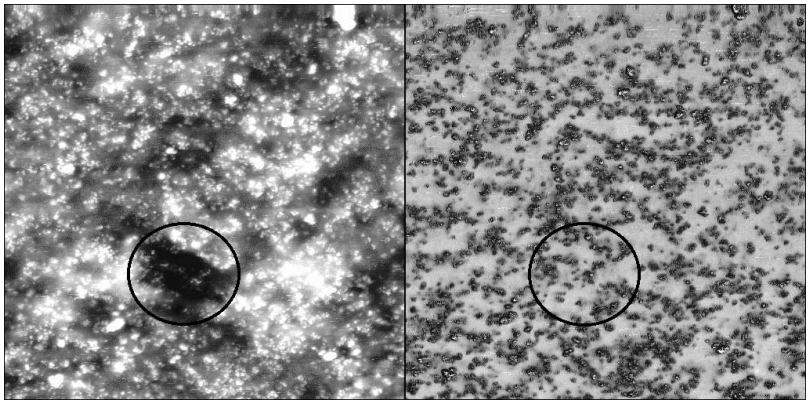

Fig. 2. Height (left) and phase (right) images of the reference system, using $A_0 = 5$ V (70 nm) and $r_s = 0.64$ ($\omega_0 = 331$ kHz).

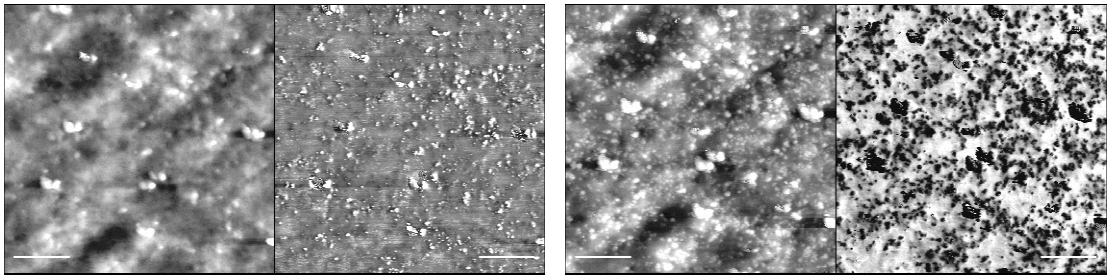

Fig. 3. Height and phase images of the reference system, using (a) $A_0 = 5$ V (70 nm), (b) $A_0 = 4$ V (55 nm), and $d_s = 2.5$ V ($\omega_0 = 310$ kHz). (The horizontal bar corresponds to 1 μm.)

glass transition temperature of the matrix ($T_g = -123$°C for PDMS) was avoided. The thin sections obtained were about 100 to 200 nm thick.

3. Results and discussion about the influence of imaging parameters on phase contrast

Fig. 1 shows typical height and phase contrasts for the reference network filled with 40 phr A300-t, in standard conditions ($\omega_0 = 324$ kHz, $A_0 = 5$ V, $r_s = 0.38$). The height image shows unambiguously silica structures as elevations, which appear bright on this image. The phase contrast is more difficult to understand. The matrix forms a uniform bright background and silica may appear dark or very bright. In this latter case, it corresponds to the structures, which are at the extreme surface of the sample considering the height image. Nevertheless, the assignment of the different domains to the matrix and the silica is unambiguous, since the structures assigned to silica particles have the expected fractal shape and size according to the image analysis. On the whole, there is a good connection between the height and phase images. But the phase image is more reliable to consider than the height image. For example, the height image in Fig. 2 reveals some irregularities to which the phase detection is not sensitive: the phase image shows silica structures, even in the holes (circle on Fig. 2) or on the bumps of the topography. Moreover, the phase image provides a better resolution than the height image. Nevertheless, the phase contrast is very sensitive to various factors affecting the tip-sample force. First, Fig. 3a and b show the same region of the reference system, imaged with the same value of $d_s = (A_0 - A_s)$, but with two different values of A_0: the phase contrast undergoes a complete reversal. Fig. 4 corresponds to the same system imaged with a greater value of A_s (or r_s) than Fig. 1: the height and phase images show completely different contrasts from those of Fig. 1. Fig. 5 points out that an increase in the cantilever stiffness ($\omega_0 = 386$ kHz) causes a significant change in the phase image contrast, compared to Fig. 1. Finally, Fig. 6 shows the images obtained on a system filled with 20 phr A300-t in the same conditions as Fig. 1 for the reference system. The two samples differ from their macroscopic moduli. In this section, we will study more precisely each of these factors affecting the contrast of height and phase images.

3.1. Dependence of image contrast on A_0

At first was proposed an analytical expression of the tip-sample force f of the following type [4], where the notations have the same signification as above:

$$f = (A_0 - A_s)\frac{k}{Q}. \tag{4}$$

According to this relationship, for the same tip and

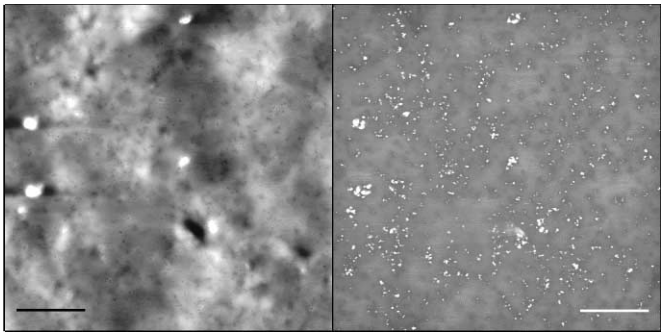

Fig. 4. Height and phase images of the reference system, using $A_0 = 5$ V (70 nm) and $r_s = 0.64$ ($\omega_0 = 324$ kHz).

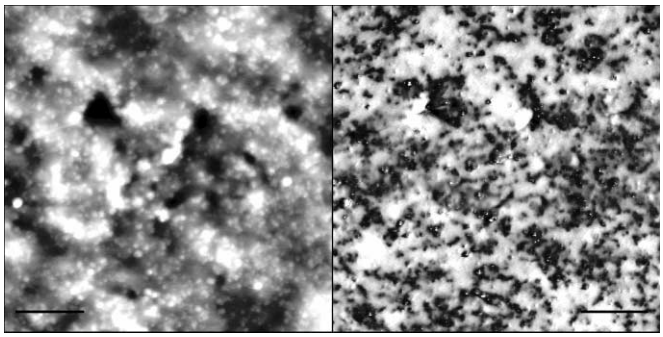

Fig. 5. Height and phase images of the reference system, using $A_0 = 5$ V (70 nm) and $r_s = 0.38$ ($\omega_0 = 386$ kHz).

cantilever, the force should be controlled by the only $d_s = (A_0 - A_s)$ value, and so should be the phase contrast. But Fig. 3a and b give the evidence that, even if the d_s value remains constant, the phase image can undergo a contrast reversal when A_0 is decreased from 5 to 4 V (which corresponds to a decrease of r_s from 0.5 to 0.38). Thus, d_s cannot be considered as a good parameter to control the tip-sample force and the phase contrast. Fig. 3a corresponds to a low tip-sample force, showing the silica structures in bright contrast. With these experimental conditions (large A_0 and large r_s) and according to Eq. (3), the phase contrast is dominated by the contribution of the local modulus. As A_0 diminishes, the contact time between the tip and the sample surface becomes longer. Thus, the contribution of the contact area becomes predominant over that of the modulus, explaining the phase contrast reversal observed in Fig. 3b. Most of the phase images show the silica structures in dark contrast and the silicone matrix in bright contrast. For these types of images, at a constant value of d_s, a decrease in A_0 causes an increase in the contact time, then in the indentation depth and eventually in the phase difference between the silica domains and the matrix (Fig. 7a and b). On the contrary, when the r_s parameter remains constant and A_0 varies, the phase contrast undergoes small variations (Fig. 8), indicating that r_s *is the main parameter controlling the tip-sample force*. This is in agreement with the other studies about the phase contrast variations [9,13].

3.2. Dependence of image contrast on r_s

In this part, all the images were recorded with the same tip and cantilever, and with free amplitude fixed at $A_0 = 5$ V (i.e. approximately 70 nm). The height and phase images for the reference sample, recorded with a cantilever of resonance frequency $\omega_0 = 331$ kHz are shown in Fig. 9. At hard tapping ($r_s = 0.38$ — Fig. 9a), the height image clearly reveals structures in bright contrast, corresponding to silica aggregates or agglomerates. At moderate tapping ($r_s = 0.5$ — Fig. 9b), the height contrast is not significantly modified whereas the phase contrast begins to reverse. At light tapping ($r_s = 0.64$ — Fig. 9c), the height contrast diminishes and some height anomalies (silica structures in weak, dark contrast) appear [9]. The phase image undergoes a radical contrast change. Now the matrix appears in dark contrast and silica in bright contrast. Moreover, as the tip-sample interaction is reduced, the indentation depth is reduced too, so the amount of silica detected diminishes; at light tapping, only the silica present at the extreme surface appears on the phase image.

At light tapping ($r_s = 0.64$ — Fig. 9c), the phase image is sensitive to the local modulus, then the stiff regions are likely to provide a greater phase shift than the compliant region. When the tip-sample force increases, i.e. when r_s diminishes, the contribution of the contact area in Eq. (3) becomes significant. For the smaller value of r_s ($r_s = 0.38$ — Fig. 9a), the phase contrast can reverse,

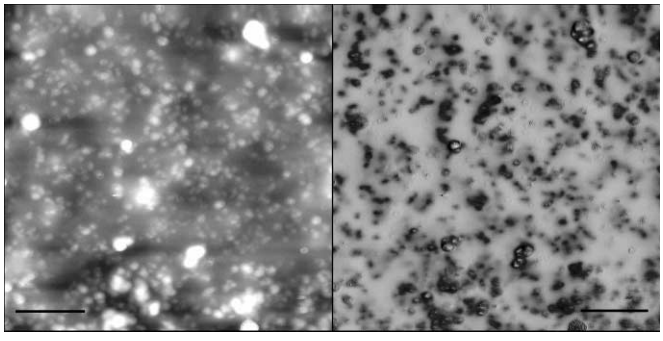

Fig. 6. Height (left) and phase (right) images of a network filled with 20 phr treated silica, using $A_0 = 5$ V (70 nm) and $r_s = 0.38$ ($\omega_0 = 324$ kHz).

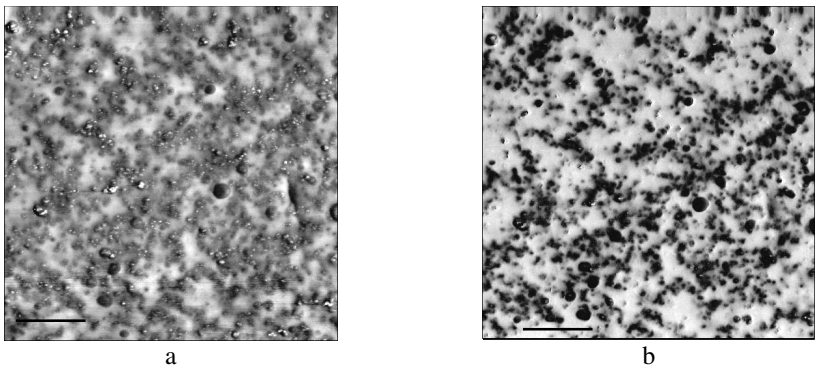

Fig. 7. Phase images of the reference system, using $d_s = 2.5$ V ($\omega_0 = 329$ kHz) and (a) $A_0 = 5$ V (70 nm), (b) $A_0 = 4$ V (55 nm). (The horizontal bar corresponds to 1 μm.)

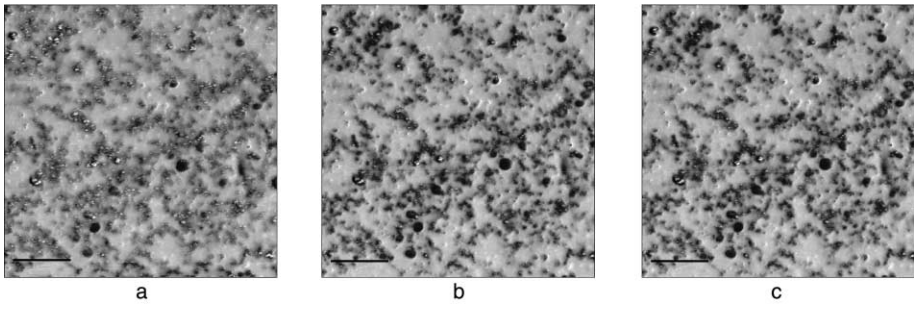

Fig. 8. Phase images of the reference system, using $r_s = 0.38$ ($\omega_0 = 329$ kHz) and (a) $A_0 = 5$ V (70 nm), (b) $A_0 = 4$ V (55 nm), (c) $A_0 = 3$ V (40 nm). (The horizontal bar corresponds to 1 μm.)

the matrix now corresponding to the bright domains and the silica to the dark ones. In this case, the contribution of the contact area probably dominates over that of the modulus in Eq. (3). Then the compliant region now provides a greater phase shift than do the stiff domains.

3.3. Dependence of image contrast on cantilever stiffness (or resonance frequency)

Fig. 10 shows the images obtained at different r_s values using a softer cantilever of resonance frequency

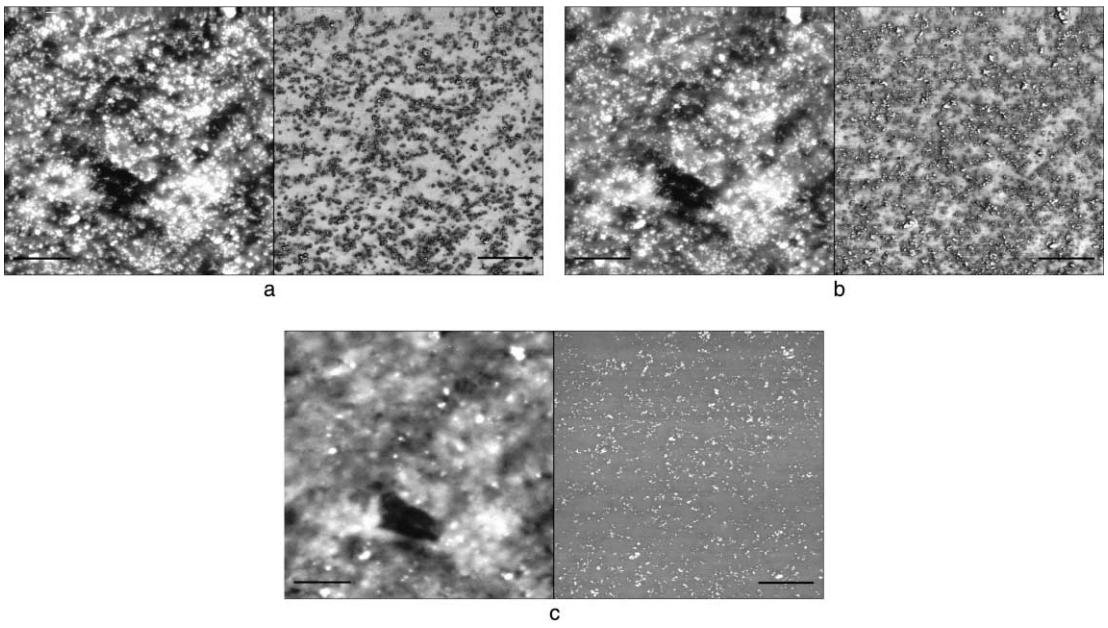

Fig. 9. Height and phase images of the reference system ($\omega_0 = 331$ kHz), using $A_0 = 5$ V (70 nm) and (a) $r_s = 0.38$, (b) $r_s = 0.5$, (c) $r_s = 0.64$. (The horizontal bar corresponds to 1 μm.)

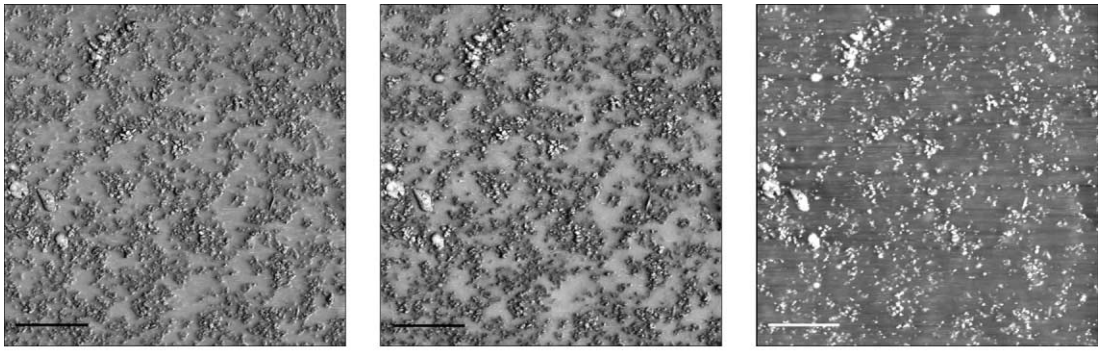

Fig. 10. Phase images of the reference system, using $A_0 = 5$ V (70 nm) and (a) $r_s = 0.38$, (b) $r_s = 0.5$, (c) $r_s = 0.64$ ($\omega_0 = 301$ kHz). (The horizontal bar corresponds to 1 μm.)

$\omega_0 = 301$ kHz and Fig. 11 with a stiffer cantilever of resonance frequency $\omega_0 = 382$ kHz. At hard tapping ($r_s = 0.38$ — Figs. 9a, 10a and 11a), the phase contrast difference between the matrix and the silica is enhanced as the cantilever stiffness becomes greater. When the cantilever stiffness is increased, the indentation force is enhanced and the contact area increases, causing an increase of the phase contrast difference between the matrix and the filler. At light tapping ($r_s = 0.64$ — Figs. 9c and 10c), the phase contrast difference between the matrix and the filler diminishes when the cantilever stiffness is increased. For the softer cantilever ($\omega_0 = 301$ kHz) and at light tapping ($r_s = 0.64$), the contribution of the modulus clearly dominates, the matrix appearing in dark contrast and silica in bright contrast. For a stiffer cantilever in the same conditions, the indentation force becomes greater and the contribution of the contact area becomes significant, reducing and even beginning to reverse the phase contrast.

3.4. Dependence of image contrast on sample macroscopic modulus

Fig. 12 shows the images obtained with the same experimental conditions ($\omega_0 = 325$ kHz, $A_0 = 5$ V, $r_s = 0.38$) on three different samples. Fig. 12a corresponds to a sample filled with 20 phr A300-t, Fig. 12b to the reference system, and Fig. 12c to a sample filled with 20 phr A300. These samples have the following Young's moduli: 0.7, 1.2 and 1.4 MPa, respectively. For the softest sample (Fig. 12a), the phase image shows two domains, the matrix in bright contrast and silica in dark contrast. For the other samples of greater moduli, the phase image shows the so-called three-levels contrast. The lower the sample macroscopic modulus, the greater the tip indentation, and hence, the more the contact area would predominate. That is why for the softest sample the matrix appears bright and the silica dark in the phase image. As the sample modulus increases with regard to the cantilever stiffness, the influence of the modulus becomes predominant, causing locally an inversion of the phase contrast for the parts of the filler structure lying at the extreme surface.

3.5. Concluding remarks

This study shows that, in TMAFM phase images of filled rubbers such as silica-filled silicone elastomers, the relative contrast of the matrix and silica depends sensitively on several factors, especially on the r_s value, which can be considered as the main parameter controlling the tip-sample force. The dependence of phase shift on r_s can be qualitatively understood

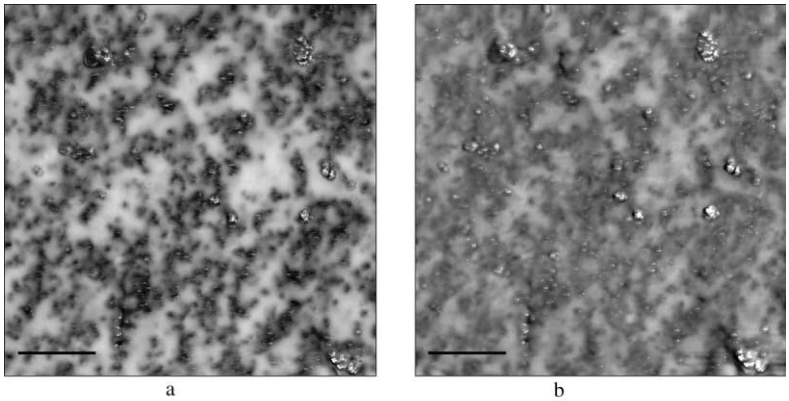

Fig. 11. Phase images of the reference system, using $A_0 = 5$ V (70 nm) and (a) $r_s = 0.38$, (b) $r_s = 0.5$ ($\omega_0 = 382$ kHz).

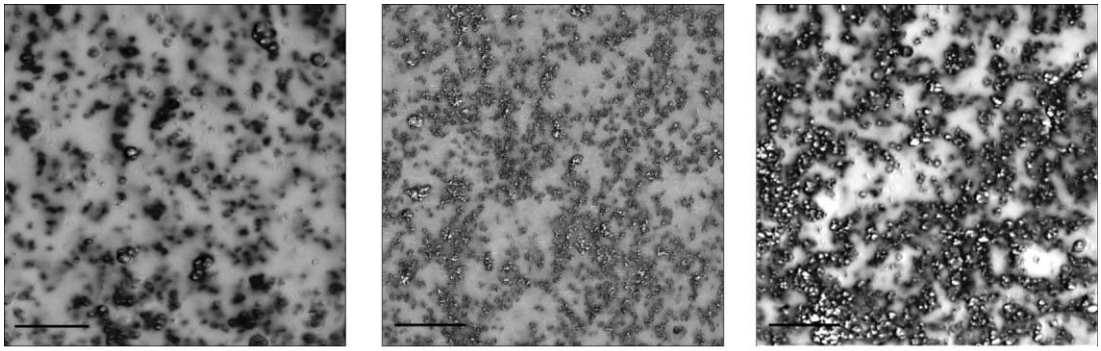

Fig. 12. Phase images using $A_0 = 5$ V (70 nm) and $r_s = 0.38$ ($\omega_0 = 325$ kHz) of (a) a network filled with 20 phr A300-t, (b) the reference system (filled with 40 phr A300-t), (c) a network filled with 20 phr A300 (untreated silica).

considering the theory of Magonov and coworkers. The phase contrast depends also on the relative stiffness of the cantilever compared to the sample modulus. A decrease in the sample modulus or an increase in the cantilever stiffness causes an enhancement of the tip indentation. This has qualitatively the same effect as a diminution of r_s. Thus, in characterizing filled elastomers by TMAFM, it is necessary to record height and phase images by systematically varying the r_s value. Otherwise, the interpretation of observed image features may be deceptive. *The control of the phase contrast is essential for any quantitative exploitation of the images, as will be shown in the following section.*

4. Discussion on the AFM potential for the characterization of silica dispersion and distribution in a silicone matrix

The silica dispersion is the result of its mixing in the PDMS gum before crosslinking. Thus, before any analysis of the crosslinked filled samples, it is useful to know more about the morphology of the alone silica. For this purpose, silica was dispersed by sonicating in a solvent and was observed by TEM. The beam transmission depends on the material: the silica structures appear darker in the bright-field images. Fig. 13 shows the dispersion of A300 silica (Fig. 13a) and A300-t silica (Fig. 13b). For both silicas, the dispersion by sonication leads to the ultimate aggregate size. The smallest aggregates have an average size of 30–40 nm, and are composed of 10–20 elementary particles.

4.1. Qualitative characterization

Concerning the A300-t silica, the AFM phase image shows some individual aggregates and some agglomerates, which have an open structure and are made of a few aggregates (Fig. 14a). These observations are in good agreement with the observations made by TEM (Fig. 14b). Note that the isolated particles on Fig. 14a are not elementary particles, but aggregates seen by their top. Concerning the untreated A300 silica, some dense agglomerates, which size can reach 1 μm, can be seen on Fig. 15. The smallest size of aggregates seen on the images is about 30–50 nm for both the A300 and the A300-t silicas, which is in agreement with the ultimate size determined by sonication. Therefore, the phase image allows the differentiation between the dispersion states of a treated silica and an untreated one.

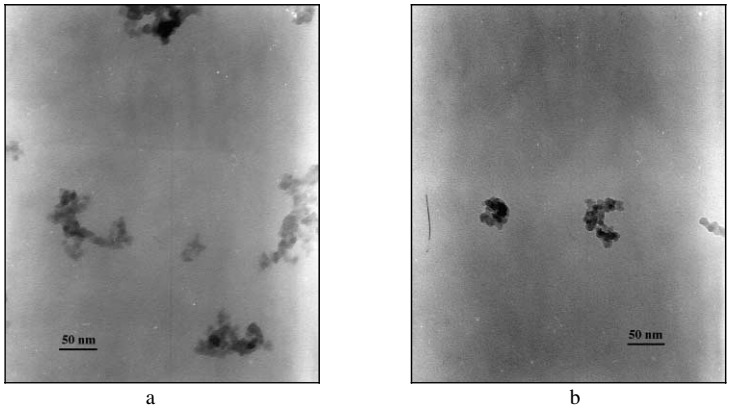

Fig. 13. TEM images of the dispersion of untreated silica A300 (a) and treated silica A300-t (b) after sonication in a solvent.

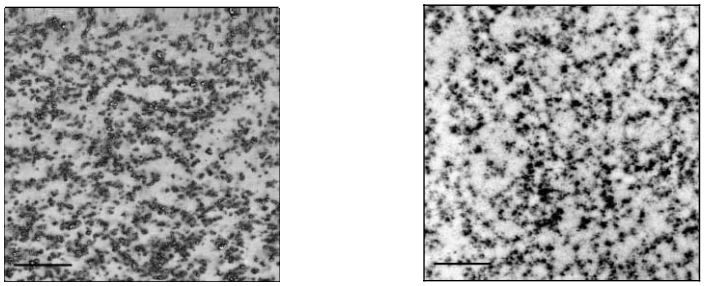

a b

Fig. 14. AFM phase image (a) and TEM image (b) of a network filled with 40 phr A300-t. The conditions used for the AFM image are: $\omega_0 = 331$ kHz, $A_0 = 5$ V and $r_s = 0.38$. (The horizontal bar corresponds to 1 μm.)

4.2. Quantitative analysis

4.2.1. Analysis method

4.2.1.1. AFM. The analysis was performed on a Macintosh computer using the public domain NIH Image program, developed at the US National Institutes of Health and available on the Internet at http://rsb.info.nih.gov/nih-image/. For the analysis, we used the so-called 'vectors method' [3]. First, the phase image is binarized (Fig. 16b). The apparent fraction of silica is then given by the percentage of black zones. Then, parallel lines are drawn on the binary image ('vectors'), in a given direction (Fig. 16c). The distance between two black zones gives an interparticle distance. The binary image contrast is reversed to determine the average particle size: the particles appear white, and their size is then given by the distance between two black zones (Fig. 16d). It is important to note that the average interparticle distance obtained by this method is not a distance between closest neighboring particles. Thus, this average distance is always much larger than the one calculated for a regular packing of particles. In order to perform a statistical treatment and to obtain average values, about 10 images were analyzed for each sample. As shown in Table 1, the values obtained are sensitive to the phase contrast that is to say to the imaging parameters. For instance, when r_s increases, the other parameters remaining constant, the tip-sample interaction decreases. Thus, the apparent fraction of silica decreases, while the interparticle distance increases.

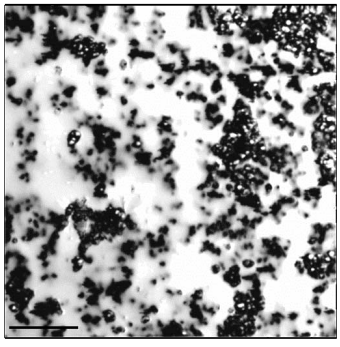

Fig. 15. AFM phase image of a network filled with 20 phr A300 ($\omega_0 = 318$ kHz,$A_0 = 5$ V and $r_s = 0.38$).

The size of particles decreases slightly: at low tip-sample interaction ($r_s = 0.64$), the phase image shows mainly the top of the silica structures. To get quantitative and reliable results, one has to find the experimental conditions to always obtain the same phase contrast. For a given sample and a given tip/cantilever set, it means working at a given r_s value (3 last rows of Table 1). If one wants to compare two samples of different moduli, the experimental parameters (cantilever stiffness and r_s value) must be adjusted in order to obtain phase images with similar contrasts.

4.2.1.2. TEM. The analysis method for TEM images presented here is the one usually performed by RHODIA Recherches, using the image analysis system Matra Pericolor 3100. The first step is an homogenization procedure of the image background, which is often heterogeneous because of the non-uniformity of the section. The second step is a binarization of the image. Then, a granulometric analysis is performed on the binary image. However, the usual methods of analyzing particle by particle cannot be performed since, in an interconnected silica network, a single particle cannot be defined. Nevertheless, the granulometric analysis is still possible by using the methods of mathematical morphology. More precisely, the method of granulometry by linear erosion is used in this case. The principle of the mathematical morphology is to probe a set with a structural element of

Table 1
Sensitivity of apparent fraction of silica, average particle size and average interparticle distance on imaging parameters

Imaging parameters	Apparent fraction of silica	Average particle size (nm)	Average interparticle distance (nm)
$A_0 = 4$ V $r_s = 0.38$ $\omega_0 = 310$ kHz	0.18	60	230
$A_0 = 5$ V $r_s = 0.5$ $\omega_0 = 310$ kHz	0.09	40	360
$A_0 = 5$ V $r_s = 0.38$ $\omega_0 = 324$ kHz	0.20	60	250
$A_0 = 5$ V $r_s = 0.5$ $\omega_0 = 324$ kHz	0.15	50	300
$A_0 = 5$ V $r_s = 0.64$ $\omega_0 = 324$ kHz	0.04	40	570
$A_0 = 5$ V $r_s = 0.5$ $\omega_0 = 382$ kHz	0.20	80	180
$A_0 = 5$ V $r_s = 0.5$ $\omega_0 = 301$ kHz	0.10	40	340
$A_0 = 5$ V $r_s = 0.38$ $\omega_0 = 329$ kHz	0.16	60	290
$A_0 = 4$ V $r_s = 0.38$ $\omega_0 = 329$ kHz	0.16	60	305
$A_0 = 3$ V $r_s = 0.4$ $\omega_0 = 329$ kHz	0.16	65	330

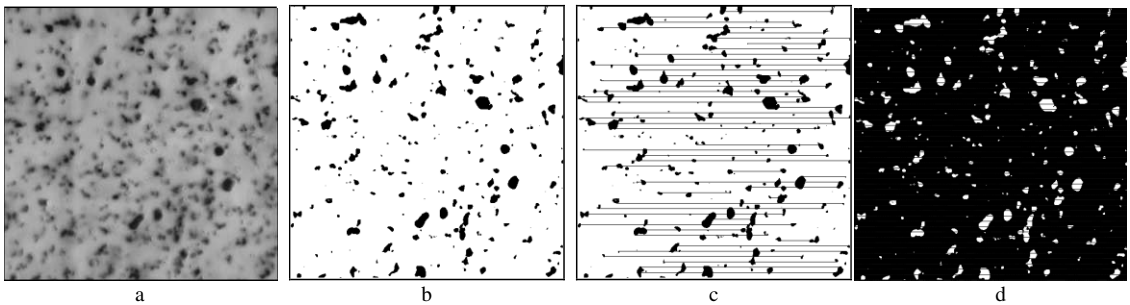

Fig. 16. Analysis of the phase image (a) by the vectors method — corresponding binary image (b) determination of the average interparticle distance (c) and of the average particle size (d).

known shape, in order to get information about the geometry and topology of the studied set [17]. The image, which is supposed to be isotropic, is binarized within two phases: silica and (silicone + PMMA). Then, erosions of the silica phase by line segments of increasing length ℓ are performed in a given direction (Fig. 17), and give access to the average size of the silica phase, which is similar to the average size of particles given by the vectors method. By the same way, erosions of the (silicone + PMMA) phase lead to the average interparticle distance d. The values of interparticle distances have to be corrected by the swelling effect due to the sample immersion in methyl methacrylate:

$$d_{\text{corrected}} = \frac{d_{\text{measured}}}{G_{\text{lin}}} = \frac{d_{\text{measured}}}{\sqrt[3]{G_{\text{vol}}}}, \tag{5}$$

G_{lin} is the linear swelling, G_{vol} is the volume swelling:

$$G_{\text{vol}} = \frac{V}{V_0} = 1 + \frac{\rho_0}{\rho_{\text{PMMA}}} \times \frac{m - m_0}{(1 - \phi_{\text{eff}})m_0}, \tag{6}$$

where ρ_0 is the density of the unfilled and unswollen network, ρ_{PMMA} is the PMMA density, m is the mass of the filled network in the swollen state, m_0 is the mass of the filled network in the unswollen state and ϕ is the silica volume fraction.

The volume swelling ratios were measured by RHODIA Recherches and are listed in Table 2.

Table 2
Volume swelling ratios in methyl methacrylate for samples of various compositions

Sample	G_{vol}
10 phr A300-t	5.40
20 phr A300-t	5.46
30 phr A300-t	5.46
40 phr A300-t	5.81
10 phr A300	5.12
20 phr A300	4.89

4.2.2. Comparison between the results obtained by AFM and TEM analysis

4.2.2.1. Apparent fraction of silica.

AFM. In Table 3 are given the apparent surface fractions of silica, obtained on AFM images, for filled networks of various A300-t loadings. According to the Delesse–Rosiwal principle, the volume fraction ϕ of a secondary phase (here the silica) in a structure (here the matrix) is equal to the surface fraction ϕ^{2D} for an idealized section of zero thickness [18]. Practically, the considered section has a finite thickness. Thus, not only particles at the surface, but also in some depth, are detected: the image shows an apparent silica fraction ϕ_{app}, which is higher than ϕ. Actually, the fractions determined on the binary images are higher than the real volume fractions. Nevertheless, the ϕ_{app} evolution with the silica loading is satisfactory: ϕ_{app} increases with the volume fraction of silica effectively introduced in the network. If the indentation depth effect was dominant, we should observe an apparent silica fraction, which increases as the material modulus decreases. The apparent fraction should then increase when the silica loading decreases. The experimental results show that it is not the case: the effect of the indentation depth is not predominant. For a distribution of monomodal spheres of radius R, ϕ_{app} and ϕ are related by the following relationship [18], where t is the analyzed thickness of the sample:

$$\phi_{\text{app}} = \frac{4R + 3t}{4R}\phi. \tag{7}$$

For the samples studied here, the dispersed particles are not spherical, but the above relationship may give a first

Table 3
Apparent fractions of silica on AFM images for various A300-t loadings

Silica loading (phr)	Young modulus (MPa)	Real volume fraction ϕ	Average apparent surface fraction ϕ_{app}
10	0.39	0.04	0.06
20	0.68	0.08	0.11
30	0.93	0.12	0.15
40	1.20	0.15	0.21

Table 4
Comparison of the values of analyzed thickness by AFM and by TEM, for various A300-t loadings

Silica loading (phr)	Young modulus (MPa)	Real volume fraction ϕ	Apparent surface fraction ϕ_{app} AFM	Analyzed thickness in AFM t_{AFM} (nm)	Fraction in the swollen state $\phi_{swollen}$	Observed apparent fraction ϕ_{app} TEM	Analyzed thickness in TEM t_{MET} (nm)
10	0.39	0.04	0.06	26	0.015	0.06	175
20	0.68	0.08	0.11	22	0.025	0.11	170
30	0.93	0.12	0.15	17	0.04	0.15	155
40	1.20	0.15	0.21	24	0.0465	0.18	150

Table 5
Average particle sizes and interparticle distances determined from AFM and TEM images on samples of various compositions

Sample	Young modulus (MPa)	ϕ	ϕ_{app} AFM	$\phi_{swollen}$	ϕ_{app} TEM	Average particle size (nm)		Average interparticle distance (nm)	
						AFM	TEM	AFM	TEM
10 phr A300-t	0.39	0.04	0.06	0.015	0.06	70	60	800	590
20 phr A300-t	0.68	0.08	0.11	0.025	0.11	80	70	550	410
30 phr A300-t	0.93	0.12	0.15	0.04	0.15	90	80	460	320
40 phr A300-t	1.20	0.15	0.21	0.045	0.18	90	80	290	220
10 phr A300	0.62	0.04	0.15	0.015	0.12	130	110	510	460
20 phr A300	1.40	0.08	0.23	0.03	0.21	110	100	290	220

approximation of the indentation depth typical of the AFM experiments. The analyzed thickness t is determined by the knowledge of ϕ and ϕ_{app} and by considering $R \approx 40$ nm. The values obtained are given in Table 4. Thus, it is verified that the indentation depth is the same for the different samples filled with various loadings of A300-t silica. It is important to note that the fact of choosing images with similar phase contrasts minimizes variations of the indentation depth. Besides, the indentation depth is about 20 nm, which seems to be reasonable, given the phase images resolution. Actually, if the indentation depth were greater, the resolution would decrease as a direct consequence (Fig. 18).

TEM. The apparent surface fraction observed on the TEM images, called ϕ_{app}, may be compared to the fraction $\phi_{swollen}$, which should be observed in the swollen state:

$$\phi_{swollen} = \frac{\phi}{G_{vol}^{2/3}}. \quad (8)$$

An analyzed thickness for the TEM experiments can then be calculated, for given $\phi_{swollen}$ and ϕ_{app} and with $R \approx 40$ nm

$$\phi_{app} = \frac{4R + 3t}{4R}\phi_{swollen} \quad (9)$$

In Table 4 are compared the analyzed thickness values for TEM and for AFM, in the case of networks filled with A300-t silica. The apparent silica fraction observed on TEM images is much higher than the fraction which should be expected by just considering the effect of swelling. The analyzed depth in TEM experiments is of the order of the thickness of the microtome section (160 nm): TEM analyzes the whole volume of the section. Thus, the analyzed depth in AFM is significantly smaller than the one analyzed in TEM.

4.2.2.2. Average particle size. In Table 5 are listed the average particle sizes determined on the AFM images and on the TEM images, for various samples. Basically, there is a good agreement between the sizes determined by the two techniques. Nevertheless, the AFM sizes are always slightly greater than the TEM sizes. This is due to the AFM resolution, which is slightly inferior to the TEM resolution. The AFM resolution is dramatically dependent on the quality of the tip.

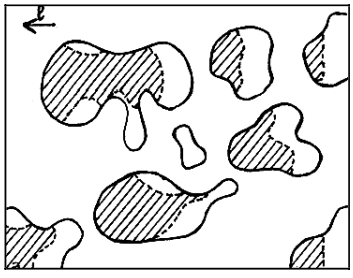

Fig. 17. Erosion of a set of particles by a line segment of length ℓ, from right to left.

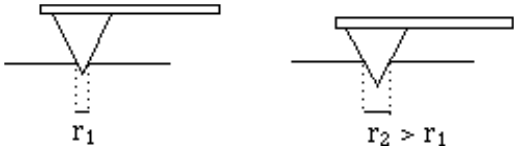

Fig. 18. Influence of the indentation depth on the image resolution. When the indentation depth increases (right), the size of the smallest features observed increases ($r_2 > r_1$).

The average particle size tends to increase a bit when the A300-t silica loading increases, indicating a little higher agglomeration for high silica content. Besides, the quantitative analysis confirms the poorer dispersion of the untreated silica: the average particle size for A300 is at least more than 30 nm higher than the size for A300-t.

4.2.2.3. Average interparticle distance. In Table 5 are listed the average interparticle distances determined by both AFM and TEM analysis. As one must recall, for TEM, the distances have been corrected by the swelling effect. Both techniques clearly show the decrease of the average interparticle distance when the silica loading increases. However, the interparticle distances determined by TEM are systematically smaller than the distances resulting from the AFM analysis. This is mainly due to the fact that the analyzed thickness is greater for TEM than for AFM. The exploitation of the AFM and TEM images for determining the interparticle distances is somehow difficult, because the measurement of the interparticle distances is very sensitive to the analyzed depth.

5. Conclusions

The experimental results presented in this paper show the potential of AFM with phase imaging for the characterization of filled elastomers and more generally of heterogeneous systems with components of different moduli. The phase image leads to a higher resolution than the height image. Nevertheless, it requires the determination of the appropriate imaging parameters, depending on the modulus of the matrix and on the cantilever stiffness. Concerning the determination of particle sizes, this technique appears to be competitive over TEM: both techniques give quantitative results concerning the silica dispersion. Regarding the quantitative analysis of interparticle distances, AFM and TEM suffer from the similar problem of analyzed depth. Nevertheless, qualitative information about the particle distribution can be provided by both techniques, but AFM offers the advantage of avoiding any specific sample preparation.

A major interest of tapping mode AFM with phase imaging is its ability to investigate the microscopic deformation of the particle structure in filled rubbers under stretching. This aspect will be developed in a forthcoming paper.

Acknowledgements

The authors thank RHODIA Silicones for providing the samples, RHODIA Recherches for the TEM analysis, and D. Dhaler and C. Noblet for useful discussions.

References

[1] Ambacher H, Strauß M, Kilian HG, Wolff S. Kautschuk Gummi Kunststoffe 1991;44:111.
[2] Hess WM. Rubber Chem Technol 1991;64:386.
[3] Maas S, Gronski W. Kautschuk Gummi Kunststoffe 1994;47:409.
[4] Zhong Q, Innis D, Kjoller K, Elings VB. Surf Sci 1993;290(1-2):L688–92.
[5] Binggeli M, Christoph R, Hinterman HE, Colchero J, Marti O. Nanotechnology 1993;4:59.
[6] Chernoff DA. In: Proceedings of the Microscopy and Microanalysis. New York: Jones and Begell, 1995.
[7] Burnham NA, Behrend OP, Oulevey F, Gremaud G, Gallo PJ, Gourdon D, Dupas E, Kulik AJ, Pollock HM, Briggs GAD. Nanotechnology 1997;8:67.
[8] Chen J, Workman RK, Sarid D, Hörper R. Nanotechnology 1994;5:199.
[9] Magonov SN, Elings VB, Whangbo MH. Surf Sci 1997;375(2-3):L385–91.
[10] Bar G, Thomann Y, Brandsch R, Cantow HJ, Whangbo MH. Langmuir 1997;13(14):3807–12.
[11] Pickering JP, Vancso GJ. Polym Bull 1998;40:549.
[12] Brandsch R, Bar G, Whangbo MH. Langmuir 1997;13(24):6349–53.
[13] Bar G, Ganter M, Brandsch R, Delineau L, Whangbo MH. Langmuir 2000;16:5702–11.
[14] Whangbo MH, Brandsch R, Bar G. Surf Sci Lett 1998;411:L794.
[15] Bar G, Brandsch R, Whangbo MH. Langmuir 1998;14:7343.
[16] Bar G, Brandsch R, Bruch M, Delineau L, Whangbo MH. Surf Sci Lett 2000;444:L11.
[17] Coster M, Chermant JL. Précis d'analyse d'image: Presses du CNRS, 1989.
[18] Maestrini C, Merlotti M, Vighi M, Malagati E. J Mater Sci 1992;27(22):5994–6016.